Shahid Chamran University of Ahvaz

Journal of Advanced Mathematical Modeling
ISSN (print): 2251-8088, ISSN (on-line): 2645-6141
Vol. 16 No. 2 (2026), pp. 56-84.
DOI: 10.22055/jamm.2026.49066.2349

AIR POLLUTION FORECASTING IN KHORRAM ABAD USING THE MODIFIED SINC NEURAL NETWORKS

GHASEM AHMADI*

Communicated by: Sohrab Effati

Abstract. Air pollution is a pressing global challenge with severe consequences for human health and ecosystems, which underscores the need for accurate forecasting models. Traditional statistical and machine learning approaches frequently face difficulties in modeling the intricate and nonlinear patterns present in air pollution data. To overcome these limitations, this paper proposes the use of a modified Sinc neural network (MSNN) as a novel framework for time series forecasting of air pollution levels. The MSNN, inspired by Sinc numerical methods, leverages the smoothness and oscillatory properties of the Sinc function while incorporating a modification that enhances its ability to model nonlinear dependencies and temporal dynamics. A discrete-time Lyapunov-based online learning algorithm is employed to train the network, ensuring stability and convergence during parameter updates. The proposed model is evaluated on real-world datasets of air pollutants, including particulate matter (PM_{10} and $PM_{2.5}$), sulfur dioxide, nitrogen monoxide, and ozone, collected from the city of Khorramabad, Iran. Comparative results demonstrate that, despite its simple structure, the MSNN achieves superior forecasting accuracy compared to conventional neural networks, highlighting its potential as an effective and computationally efficient tool for environmental time series prediction.

MSC(2020): 68T07, 37M10.

Keywords: Air pollution, time series forecasting, modified Sinc neural network.

Received: 17 February 2025, Accepted: 17 June 2026.

*Corresponding author.

1. Introduction

Air pollution is a critical global issue that significantly affects human health, ecosystems, and the climate. Accurate prediction of air pollution levels is essential for implementing timely public health interventions and guiding effective policy decisions. Traditional prediction methods, including statistical models and conventional machine learning algorithms, frequently face difficulties in modeling the intricate and nonlinear patterns present in air pollution data. Consequently, researchers have increasingly turned to artificial neural networks (ANNs), which are well-suited for modeling complex and dynamic systems, to achieve more accurate air quality forecasting.

ANNs are inspired by the human nervous system, consisting of computational neurons interconnected through weighted edges. By adjusting these weights according to learning rules, ANNs can approximate complex nonlinear functions. Their architectures vary widely, ranging from simple feedforward networks, where information flows from input to output, to more advanced structures such as recurrent and convolutional neural networks. By leveraging these principles, ANNs have become a cornerstone of modern machine learning, capable of solving a wide range of problems that were previously considered intractable. Their ability to learn from data and generalize to unseen examples makes them indispensable in today's data-driven world.

Accurate forecasting of air pollutants has received increasing attention due to its applications in public health and urban management. Early approaches employed statistical time-series models such as ARIMA and SARIMA, or machine learning regressors such as support vector regression (SVR) and random forests. These models often required extensive feature engineering and failed to capture the nonlinear and nonstationary dynamics of pollutant time series. The rise of ANNs has led to significant improvements in predictive accuracy.

Several studies have demonstrated the utility of neural networks for air quality forecasting. For instance, Córdova et al. [11] applied ANNs for air pollution prediction in Lima, Peru. In Iran, Maleki et al. [21] predicted air pollution in Ahvaz using ANNs, while Sadeghi and Khaksar Astane [26] focused on short-term forecasts in the same city. Ghaemi et al. [15] combined fuzzy-adaptive neural networks with principal component analysis to predict air quality in Tehran. Recently, Ahmadi and Akbari applied multilayer perceptrons to predict air pollution in Lorestan Province [4].

Recurrent neural networks (RNNs), particularly long short-term memory (LSTM) and gated recurrent unit (GRU) models, were among the first widely adopted approaches for pollutant forecasting due to their ability to capture temporal dependencies. Several studies combined LSTM/GRU with decomposition techniques such as empirical mode decomposition (EMD), yielding improved results in handling nonstationary signals [19, 22]. However, these methods remained limited in scenarios where spatial dependencies between monitoring sites were critical.

To address spatial interactions, convolutional and hybrid convolutional–recurrent networks were developed. For instance, ConvLSTM and CNN–LSTM models integrate convolutional layers to extract spatial features with recurrent layers for temporal modeling. These approaches enhanced performance for multi-site forecasts, where pollutant transport and meteorological patterns are important [12]. More recent studies incorporated attention mechanisms to forecast air pollutant levels [20].

Graph neural networks (GNNs) have also gained popularity in air quality prediction. By representing monitoring stations as graph nodes, GNNs explicitly learn the spatial propagation of pollutants. When combined with temporal models, they achieve state-of-the-art performance for 24–72 hour predictions [31]. Hybrid GNN architectures with attention or dynamic graph construction further improve accuracy.

Recently, transformer-based and attention-driven architectures have been introduced for air quality forecasting. Their ability to capture long-range temporal dependencies without vanishing gradients makes them highly effective for long-term prediction. Architectures such as EMD–Transformer–BiLSTM and CNN–Transformer pipelines have demonstrated strong results, especially when multimodal data (meteorological, satellite, traffic) are incorporated [12].

Despite these advances, several limitations persist. Current deep learning models often require large parameter counts and long training times. Many lack theoretical stability guarantees for online learning, which is crucial in streaming environments. Furthermore, although spatio-temporal dependencies are modeled, frequency-domain patterns (e.g., diurnal and seasonal oscillations) are rarely captured explicitly.

The Modified Sinc Neural Network (MSNN) incorporates frequency-sensitive basis functions, providing a compact representation of oscillatory signals. The use of a discrete-time Lyapunov-based learning algorithm ensures stable online training. Thus, MSNN combines

interpretability, efficiency, and theoretical stability, making it a promising approach for air pollution time-series forecasting.

A limited number of studies have investigated Sinc Neural Networks (SNNs). Elwasif and Fausett applied SNNs with a single input and output to approximate univariate functions [14]. Other researchers have employed Sinc-based convolutional networks for EEG motor execution decoding [8] and brain–computer interface motor imagery classification [9]. Applications of SNNs also extend to speech recognition [23], speaker and age identification [24], EEG motor imagery classification [18], and human motion recognition [7]. In applied mathematics, Heydari and Ahmadi employed SNNs to solve fractional optimal control problems [16]. Recently, the author extended SNNs for chaotic system identification and weather forecasting [1, 3].

However, the standard SNN may face limitations when modeling highly nonlinear and complex systems. To overcome these challenges, the author proposed the Modified SNN (MSNN) [1], which refines the architecture to better capture nonlinear dependencies and intricate temporal dynamics. MSNN retains the advantages of the Sinc function, such as smoothness, oscillation, and band-limitation, while extending its modeling capacity. The main advantages of MSNN are:

- MSNN leverages the Sinc function to achieve comparable or superior performance with fewer parameters, reducing computational costs and memory requirements.
- It integrates seamlessly with existing neural network architectures, enhancing performance without requiring a complete redesign.
- By incorporating frequency-domain information, MSNN excels in time-series forecasting, signal processing, and other frequency-sensitive tasks.

The objective of this study is to evaluate the effectiveness of MSNN for air pollution forecasting. First, we describe the mathematical theory of time-series forecasting using MSNN, trained via a discrete-time Lyapunov-based learning algorithm. We then apply the proposed approach to forecast pollutant concentration levels.

The proposed model is tested on datasets encompassing various pollutants, including particulate matter ($PM_{2.5}$, PM_{10}), nitrogen monoxide (NO), sulfur dioxide (SO_2), and ozone (O_3). The datasets were obtained from air quality monitoring stations in Khorramabad, Iran. Its performance is benchmarked against standard SNN and multilayer

perceptron (MLP) models, with evaluation focused on forecasting accuracy and computational efficiency. Results indicate that MSNN, despite its simple structure, demonstrates strong capability in air pollution forecasting.

The remainder of this paper is organized as follows. Section 2 presents the structure of MSNN. Section 3 discusses its application in time-series prediction. Section 4 addresses the issue of air pollution forecasting. Section 5 demonstrates the use of MSNN to forecast pollutant concentration levels. Finally, Section 6 concludes the paper.

2. **Modified Sinc Neural Network (MSNN)**

This section presents the structure and learning mechanism of the proposed Modified Sinc Neural Network (MSNN).

2.1. **Sinc Function.** In the MSNN, the hidden layer employs the Sinc basis function as its activation function. The Sinc function frequently appears in signal processing and Fourier transform analysis and is sometimes referred to as the sampling function. In this study, the normalized Sinc function is defined as:

$$Sa(x) = \begin{cases} \dfrac{\sin(\pi x)}{\pi x}, & x \neq 0, \\ 1, & x = 0. \end{cases} \tag{2.1}$$

The Sinc function plays a crucial role across various fields of applied mathematics and engineering, including Sinc interpolation and numerical Sinc methods, which have shown remarkable effectiveness in solving nonlinear problems [30]. As the inverse Fourier transform of the rectangular function, it is a fundamental component in signal processing, bridging the understanding of signals in both time and frequency domains [**?**].

This function is smooth and oscillatory, alternating between positive and negative values, and gradually decays toward zero as the input tends to infinity. It also serves as the foundation of the Whittaker cardinal function, an important construct in approximation theory.

Let the i-th Sinc basis function be expressed as

$$Sa_i(x) = Sa\left(\frac{1}{h}(x - ih)\right), \quad i = -\infty, \ldots, \infty, \tag{2.2}$$

where h is a positive real number. For a real-valued function f, the Whittaker cardinal series is defined as:

$$C(f,h)(x) = \sum_{i=-\infty}^{\infty} f(ih)\, Sa_i(x), \tag{2.3}$$

which interpolates f at the discrete grid points ih $(i = -\infty, \ldots, \infty)$.

In the complex ω-plane, the strip domain D_d is given by [13]:

$$D_d = \{\omega = t + is \mid |s| < d\}. \tag{2.4}$$

When a problem is defined over a subinterval $I \subset \mathbb{R}$, a conformal mapping ϕ is introduced such that $\phi(I) = \mathbb{R}$. Let ϕ be a conformal map and ζ its inverse, mapping the simply connected domain D (which includes the interval $(0,1)$) onto D_d. Hence, for the subinterval $I = (0,1) = \zeta(\mathbb{R})$, with $\phi(0) = -\infty$ and $\phi(1) = +\infty$, the function f can be approximated as:

$$f(x) \approx \sum_{i=-N}^{N} f(x_i)\, Sa_i(\phi(x)), \tag{2.5}$$

where $x_i = \zeta(ih)$, and

$$Sa_i(x) = Sa\left(\frac{\phi(x)}{h} - i\right) \tag{2.6}$$

denotes the shifted Sinc basis function.

Based on these formulations, the following conformal mappings can be used to construct single-exponential and double-exponential Sinc approximations, respectively [13]:

$$z = \psi_1(w) \;=\; \frac{1}{2} + \frac{1}{2}\tanh\left(\frac{\pi}{2}\sinh(w)\right), \tag{2.7}$$

$$z = \psi_2(w) \;=\; \frac{1}{2} + \frac{1}{2}\tanh\left(\frac{w}{2}\right), \tag{2.8}$$

which map the real interval $(-\infty, +\infty)$ onto $(0,1)$.

2.2. **The structure of MSNN.** There has been relatively limited research devoted to neural networks employing the Sinc activation function. A notable early contribution in this area was made by Elwasif and Fausett (1996), who proposed a single-input, single-output Sinc Neural Network (SNN) for single-variable function approximation [14]. More recently, Heydari and Ahmadi extended the SNN framework to address fractional optimal control problems [16].

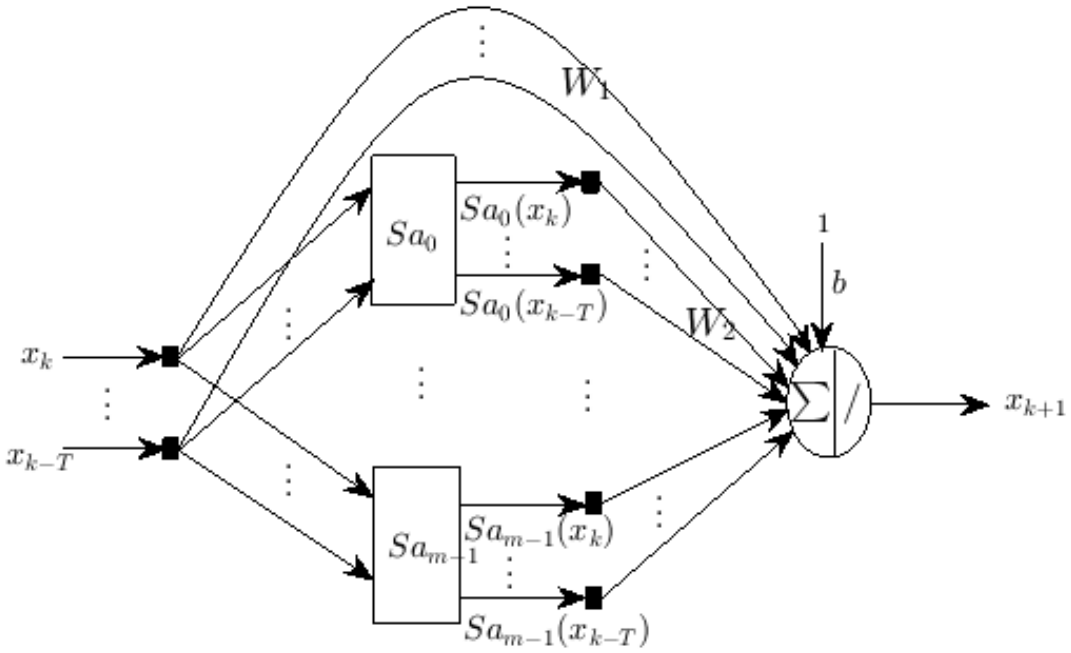


FIGURE 1. The architecture of MSNN in time series forecasting [3].

Building upon the foundational SNN models introduced in [14, 16] and incorporating the Sinc basis functions defined in equations (2.2), (2.3), and (2.5), the author developed the Modified Sinc Neural Network (MSNN) [1]. The MSNN architecture consists of three layers, where the hidden layer is composed of Sinc basis functions. In this structure, the inputs are directly connected to the outputs, and the parameters linking the input and hidden layers are assumed to be uniformly equal to one.

Let

$$X = [x_1, x_2, \ldots, x_n]^T, \quad Y = [y_1, y_2, \ldots, y_q]^T$$

denote the input and output vectors of the MSNN, respectively. Suppose that $S_i(t)$, $(i = 0, 1, 2, \ldots, m-1)$ represents the i-th Sinc basis function. Then, we define

$$\begin{aligned} Sa_i(X) &= [Sa_i(x_1), Sa_i(x_2), \ldots, Sa_i(x_n)]^T, \quad i = 0, 1, 2, \ldots, m-1, \\ \mathbf{Sa}(X) &= \begin{bmatrix} Sa_0(X) \\ Sa_1(X) \\ \vdots \\ Sa_{m-1}(X) \end{bmatrix}. \end{aligned} \tag{2.9}$$

Let W_1 denote the matrix of parameters connecting the input layer to the output layer, W_2 the matrix of parameters connecting the hidden layer to the outputs, and $\mathbf{b}$ the vector of biases associated with the output neurons. Accordingly, the network output can be expressed as:

$$\begin{aligned} Y &= W_1 X + W_2 \mathbf{Sa}(X) + \mathbf{b} \\ &= \begin{bmatrix} W_1 & W_2 & \mathbf{b} \end{bmatrix} \begin{bmatrix} X \\ \mathbf{Sa}(X) \\ 1 \end{bmatrix} \\ &= W\mathbf{S}(X), \end{aligned} \tag{2.10}$$

where

$$W = \begin{bmatrix} W_1 & W_2 & \mathbf{b} \end{bmatrix}, \qquad \mathbf{S}(X) = \begin{bmatrix} X \\ \mathbf{Sa}(X) \\ 1 \end{bmatrix}. \tag{2.11}$$

Figure 1 illustrates the schematic representation of the MSNN applied to time series prediction.

Remark 2.1. The MSNN inherits the approximation properties of Sinc expansions. In particular, for functions that are analytic in a strip around the real axis (or for sufficiently smooth functions on a compact interval), finite Sinc expansions (linear combinations of shifted and scaled Sinc basis functions) approximate the target function arbitrarily well; detailed error estimates and exponential convergence for analytic targets are available in the Sinc numerical-methods literature [30]. A Sinc neural network with a finite hidden layer of Sinc units is algebraically equivalent to a finite Sinc expansion (the hidden units implement the shifted/scaled Sinc bases and the output layer is a linear combination). Consequently, Sinc-based networks are universal approximators for this class of functions; this fact has been used constructively in earlier work on Sinc networks and demonstrated numerically [14]. We therefore assert that MSNNs have strong approximation capability for smooth and oscillatory environmental signals, which motivates their use for environmental time series forecasting.

Remark 2.2. the MSNN is introduced to enhance the flexibility and applicability of the standard SNN. The main modification lies in incorporating both linear and Sinc-basis

mappings (see Eq. 2.10), which allows the network to simultaneously capture linear trends and nonlinear oscillatory components of the data. Therefore, direct connections between the input layer and output layer are introduced, enabling the model to better approximate functions with strong linear dependencies while still exploiting the expressive power of Sinc functions. This structural modification makes MSNN more efficient and robust for modeling complex, noisy, and highly dynamic environmental time series such as air pollution data, where both smooth seasonal variations and abrupt short-term fluctuations must be represented accurately.

2.3. **Training of the MSNN.** The parameters of the MSNN are trained using an appropriate learning algorithm to obtain optimal estimates that minimize the prediction error in time series forecasting. Let Y_k denote the true output of the underlying system at time step k, corresponding to the input X_k, and let $\widehat{Y}_k$ represent the MSNN output at the same time index. The modeling error is therefore defined as:

$$E_k = Y_k - \widehat{Y}_k. \tag{2.12}$$

Following the approach outlined in [2], the weight update law for the MSNN can be expressed as:

$$\Delta W_k = \Gamma E_k \mathbf{S}(X_k)^T, \tag{2.13}$$

where Γ is a positive definite matrix containing the learning rates.

Assume that the MSNN with optimal parameters $W_\star$ can accurately represent the system output:

$$Y_k = W_\star \mathbf{S}(X_k). \tag{2.14}$$

Let W_k denote the current estimate of the optimal parameters $W_\star$. Accordingly, the MSNN output at iteration k is:

$$\widehat{Y}_k = W_k \mathbf{S}(X_k), \tag{2.15}$$

and the corresponding modeling error can be rewritten as:

$$E_k = W_\star \mathbf{S}(X_k) - W_k \mathbf{S}(X_k) = \widetilde{W}_k \mathbf{S}(X_k), \tag{2.16}$$

where $\widetilde{W}_k = W_\star - W_k$ denotes the parameter estimation error.

Theorem 2.3. *Suppose that the MSNN parameters are updated according to (2.13), and that the following condition holds:*

$$\lambda_{\max}(\Gamma)\ \max_k \|\boldsymbol{S}(X_k)\|^2 \leq 2. \tag{2.17}$$

Then, the modeling error E_k asymptotically converges to zero.

Proof. Consider the Lyapunov candidate function

$$v_k = \mathrm{tr}\left(\widetilde{W}_k^T \Gamma^{-1} \widetilde{W}_k\right).$$

Using the relation $\Delta\widetilde{W}_k = -\Delta W_k$, we obtain:

$$\begin{aligned}
\Delta v_k &= v_{k+1} - v_k \\
&= \mathrm{tr}\left(\widetilde{W}_{k+1}^T \Gamma^{-1} \widetilde{W}_{k+1}\right) - \mathrm{tr}\left(\widetilde{W}_k^T \Gamma^{-1} \widetilde{W}_k\right) \\
&= 2\mathrm{tr}\left(\widetilde{W}_k^T \Gamma^{-1} \Delta\widetilde{W}_k\right) + \mathrm{tr}\left(\Delta\widetilde{W}_k^T \Gamma^{-1} \Delta\widetilde{W}_k\right) \\
&= -2\mathrm{tr}\left(\widetilde{W}_k^T E_k \mathbf{S}(X_k)^T\right) + \mathrm{tr}\left(\mathbf{S}(X_k) E_k^T \Gamma E_k \mathbf{S}(X_k)^T\right) \\
&= -2\mathrm{tr}\left(\widetilde{W}_k^T \mathbf{S}(X_k) E_k^T\right) + E_k^T \Gamma E_k \mathbf{S}(X_k)^T \mathbf{S}(X_k) \\
&= -2\mathrm{tr}\left(E_k E_k^T\right) + E_k^T \Gamma E_k \|\mathbf{S}(X_k)\|^2 \\
&\leq -2\|E_k\|^2 + \lambda_{\max}(\Gamma)\|E_k\|^2 \|\mathbf{S}(X_k)\|^2 \\
&\leq -2\|E_k\|^2 + \left(\lambda_{\max}(\Gamma) \max_k \|\mathbf{S}(X_k)\|^2\right) \|E_k\|^2 \\
&= \left(\lambda_{\max}(\Gamma) \max_k \|\mathbf{S}(X_k)\|^2 - 2\right) \|E_k\|^2 \qquad (2.18)
\end{aligned}$$

From (2.17), it follows that $\Delta v_k < 0$, indicating that the sequence $\{v_k\}$ is monotonically decreasing. Since v_k is positive definite and bounded below, it converges to a finite limit:

$$\lim_{k\to\infty} v_k = v_\infty < \infty. \tag{2.19}$$

Therefore,

$$\begin{aligned}
0 &< \left(2 - \lambda_{\max}(\Gamma) \max_k \|\mathbf{S}(X_k)\|^2\right) \sum_{k=0}^{\infty} \|E_k\|^2 \\
&\leq -\sum_{k=0}^{\infty} \Delta v(k) = v_0 - v_\infty < \infty. \qquad (2.20)
\end{aligned}$$

Consequently, $\{E_k\} \in \ell^2$. By applying the discrete version of Barbalat's lemma [17], we conclude that:

$$\lim_{k\to\infty} E_k = 0. \tag{2.21}$$

□

The convergence of the proposed MSNN training algorithm is ensured by adopting a discrete-time Lyapunov stability framework. Specifically, the Lyapunov candidate function is constructed based on the weight estimation error, which measures the deviation between the actual weights and their optimal values. By showing that the difference of this Lyapunov function across successive training iterations is always non-increasing, we establish that the parameter updates remain stable and the error converges asymptotically toward a bounded neighborhood of zero. This analysis guarantees that the MSNN does not exhibit divergence or oscillatory instability during online learning, a property often lacking in conventional neural networks trained with gradient-based algorithms. The inclusion of both linear and Sinc basis mappings further supports convergence, since the richer function space reduces approximation error and accelerates the descent of the Lyapunov function.

3. **Time Series Forecasting Using MSNN**

Time series forecasting involves predicting future observations based on previously recorded data. This methodology plays a crucial role in various fields such as finance, meteorology, environmental monitoring, and supply chain management. In recent years, ANNs have gained considerable attention for their ability to model nonlinear and complex temporal dependencies, leading to improved forecasting accuracy [5].

A time series can be expressed as a sequence of data points $\{x_k\}_{k=0}^{\infty}$, where x_k denotes the observed value at discrete time index k. The goal is to estimate the next value x_{k+1} using a set of preceding observations. Let the relationship between x_{k+1} and the past values $x_k, x_{k-1}, \ldots, x_{k-T}$ be represented by a nonlinear function f:

$$\begin{aligned} x_{k+1} &= f(x_k, x_{k-1}, \ldots, x_{k-T}) \\ &= f(X_k), \end{aligned} \tag{3.1}$$

where $X_k = [x_k, x_{k-1}, \ldots, x_{k-T}]^T$ represents the input vector at time k.

Assume that A is a Hurwitz matrix, meaning all its eigenvalues lie strictly inside the unit circle. By adding and subtracting the term AX_k on the right-hand side of (3.1), we obtain:

$$x_{k+1} = AX_k + g(X_k), \tag{3.2}$$

where $g(X_k) = f(X_k) - AX_k$ denotes the nonlinear component.

To approximate the nonlinear function $g(\cdot)$, we employ the MSNN model defined in (2.10), yielding:

$$x_{k+1} = AX_k + W_\star \mathbf{S}(X_k), \tag{3.3}$$

where $W_\star$ denotes the optimal weight matrix of the MSNN.

Accordingly, the parametric representation of the forecasting model can be expressed as:

$$\widehat{x}_{k+1} = AX_k + \widehat{W}_k \mathbf{S}(X_k), \tag{3.4}$$

where $\widehat{x}_{k+1}$ is the predicted output of the MSNN at time $k+1$, and $\widehat{W}_k$ denotes the estimate of the optimal parameter matrix $W_\star$ at time step k.

Remark 3.1. Eq. (3.3) defines the ideal nonlinear autoregressive model with unknown optimal parameters $W_\star$, while Eq. (3.4) defines the parametric approximation realized by the MSNN during training, where $\widehat{W}_k$ approximates $W_\star$.

The primary role of the MSNN in this study is to serve as an effective tool for time series forecasting of air pollutant concentrations. Unlike conventional feedforward networks that approximate nonlinear mappings in a purely data-driven manner, the MSNN leverages the oscillatory and smooth characteristics of Sinc basis functions, which are well suited for modeling the periodic and seasonal behaviors typically observed in environmental time series. By incorporating a discrete-time Lyapunov-based learning algorithm, the MSNN not only achieves stable online adaptation to streaming pollution data but also ensures convergence of the training process, an aspect often missing in standard neural architectures. This dual capability allows MSNN to capture both short-term fluctuations (e.g., sudden spikes in $PM_{2.5}$ due to local emissions) and long-term temporal dependencies (e.g., seasonal variations in ozone levels), thereby improving predictive accuracy.

The convergence of the proposed MSNN training algorithm is ensured by adopting a discrete-time Lyapunov stability framework [1, 6]. Specifically, the Lyapunov candidate function is constructed based on the weight estimation error, which measures the deviation between the actual weights and their optimal values. By showing that the difference of this Lyapunov function across successive training iterations is always non-increasing, we establish that the parameter updates remain stable and the error converges asymptotically toward a bounded neighborhood of zero. This analysis guarantees that the MSNN does not exhibit divergence or oscillatory instability during online learning, a property often lacking in conventional neural networks trained with gradient-based algorithms. The inclusion of both linear and Sinc basis mappings further supports convergence, since the richer function space reduces approximation error and accelerates the descent of the Lyapunov function.

In terms of computational complexity, the MSNN maintains an efficiency level comparable to that of traditional feedforward neural networks. As shown in Tables 2–6, the number of trainable parameters in the MSNN is relatively small, which makes its training process computationally inexpensive. This complexity is similar to that of a single hidden-layer MLP; however, due to the high representational capacity of the Sinc basis functions, MSNN typically requires fewer hidden neurons to achieve comparable or superior accuracy. Consequently, the overall training time is shorter, and memory usage is significantly lower compared to deeper architectures such as LSTM or CNN, which rely on recurrent or convolutional computations with higher computational overhead. Therefore, the MSNN provides a favorable balance between accuracy, stability, and computational efficiency, making it particularly well-suited for real-time forecasting of environmental time series data.

4. **Air pollution forecasting**

Air is a natural blend of chemical elements, predominantly nitrogen and oxygen. However, in densely populated or industrialized areas, the composition of air is significantly altered due to the presence of additional chemical compounds, collectively referred to as pollutants. These pollutants originate from both natural phenomena, such as volcanic eruptions and forest fires, and human activities, including industrial emissions, vehicular

exhaust, and waste burning. Pollutants may also form through complex chemical reactions in the atmosphere, often catalyzed by sunlight or specific environmental conditions [4].

Among these, particulate matter poses severe risks to human health. High concentrations of PM_{10} can cause respiratory distress and lead to increased hospitalization rates, while $PM_{2.5}$ is strongly associated with cardiovascular and pulmonary diseases. Particles larger than 10 microns are generally filtered out by the upper respiratory system, preventing deeper penetration. Ozone is another significant pollutant, with its harmful effects dependent on its altitude. Stratospheric ozone protects the Earth from harmful ultraviolet rays, whereas ground-level ozone, a product of photochemical reactions during sunny weather, peaks during the afternoon and is primarily a summer pollutant [29]. Nitrogen monoxides (NO), is a critical air pollutant, and can cause severe respiratory issues [32]. SO_2, a gas with a sharp, irritating odor, reacts with other particles in the atmosphere, exacerbating air pollution's harmful effects.

Dust storms are another major source of air pollution, particularly in regions with arid and semi-arid climates. Iran, with its vast desert areas, is especially vulnerable. Neighboring countries like Iraq, Saudi Arabia, and Syria, which also have extensive deserts, contribute to the dust transported into Iran by winds such as the *Shamal wind* [25]. Western regions of Iran, including Khorram Abad, experience the brunt of these dust storms. The increased desertification has made air pollution in Khorram Abad and its neighboring regions a pressing issue that requires immediate intervention and mitigation strategies.

Timely forecasting of air pollution is crucial for minimizing its adverse effects. Numerous predictive models have been developed, such as the multiscale air quality association model [10] and the chemistry-coupled climate research and forecasting model [27]. However, many traditional models struggle with accuracy and adaptability. In contrast, artificial neural networks (ANNs) have emerged as powerful tools for air quality modeling and time series forecasting. They excel at capturing nonlinear relationships within environmental data, making them ideal for predicting pollutant levels.

We use the knowledge discovery from databases (KDD) method to pull out and study details about air pollutants and their predictions. The main goal of KDD is to find new and possibly useful insights from the raw data kept in databases [11]. This approach allows

for forecasting air quality several hours ahead, which can help in making decisions for city management. The KDD process consists of these stages: (a) examining the phenomenon, (b) studying the data, (c) preprocessing the data, (d) creating models, and (e) evaluating the results. Each part of this process is explained in the sections that follow.

- Examining the phenomenon: The initial step involves exploring the issue of air pollution in Khorram Abad city, focusing on forecasting air quality to assist in formulating pollution reduction policies. We utilize MSNN to predict pollutant levels in the coming hours. Khorram Abad is situated in southwestern Iran. Given the issue of fine dust and the city's proximity to the western borders and the deserts of Iraq, Saudi Arabia, and Syria, air pollution is a significant concern. Khorramabad, with a population exceeding 400,000, is encircled by the Zagros mountains, which likely leads to pollutant accumulation. Additionally, the presence of various pollution sources makes air quality a critical issue in this city.
- Studying the data: We focus on data collected from air quality monitoring stations in Khorramabad. The data, recorded hourly from early 2015 to December 2023, includes pollutants such as $PM_{2.5}$, PM_{10}, NO, SO_2, and O_3. However, the dataset suffers from significant gaps and inaccuracies, complicating the modeling process. To address these issues, we employ various methods, which are discussed in subsequent sections. Figure 3 displays the hourly raw data from the air quality monitoring station at Lorestan University of Medical Sciences from April 1, 2015, to December 20, 2023.
- Data Preprocessing: The data must undergo preprocessing before it can be used for predictions. This preparation involves several steps. Real-world air quality datasets often suffer from measurement errors, missing sensor readings, and irregular sampling intervals. Therefore, before training the models, the raw dataset was carefully examined, and a cleaning procedure was applied to identify missing and corrupted values. For the Khorramabad dataset, the proportion of missing values varied across pollutants due to sensor downtime and communication issues. These missing values were imputed using a linear interpolation, followed by smoothing to remove residual noise. To further evaluate robustness, controlled levels of noise with SNR=35 were added to the dataset. The MSNN maintained stable performance under these perturbations, with only a modest increase in mean squared

error (MSE) compared to the clean data scenario. For smoothing the data, a butterworth filter ($\omega = 0.05$) is utilized. Table 1 summarizes the data quality statistics after data imputation.

TABLE 1. Summary of missing data for pollutant concentrations in Khorramabad dataset.

Pollutant	Missing Data (%)	Interpolated (%)	Final Usable Data (%)
$PM_{2.5}$	1	1	100
PM_{10}	0.2	0.2	100
NO	24	16	92
SO_2	20	12	92
O_3	34	19	85

The dataset from monitoring stations is composed of a series of observations x_k recorded at time k, with data collected at hourly intervals. Additionally, some data requires balancing. We define approximate limits for each variable and replace any values that fall outside these limits with the predefined bounds. Figure 2 illustrates the air pollution data after applying these preparation operations. Next, we normalize all data to the range $[0, 1]$ using the following formula:

$$y_k = \frac{x_k - \min_k\{x_k\}}{\max_k\{x_k\} - \min_k\{x_k\}}$$

Here, y_k represents the normalized value at time index k, x_k is the observed value at time index k, $\min_k\{x_k\}$ is the minimum value, and $\max_k\{x_k\}$ is the maximum value in the dataset. To smooth the time series, we calculate the average of five consecutive data points and make predictions based on this smoothed series. Additionally, we apply a filter to create a dataset with a relatively smooth curve.

- Creating models: In this work, MSNN is utilized as the neural model for air pollution forecasting. This neural model is trained using an online learning algorithm based on the Lyapunov stability theory. Hyperparameters are adjusted empirically to improve model performance.

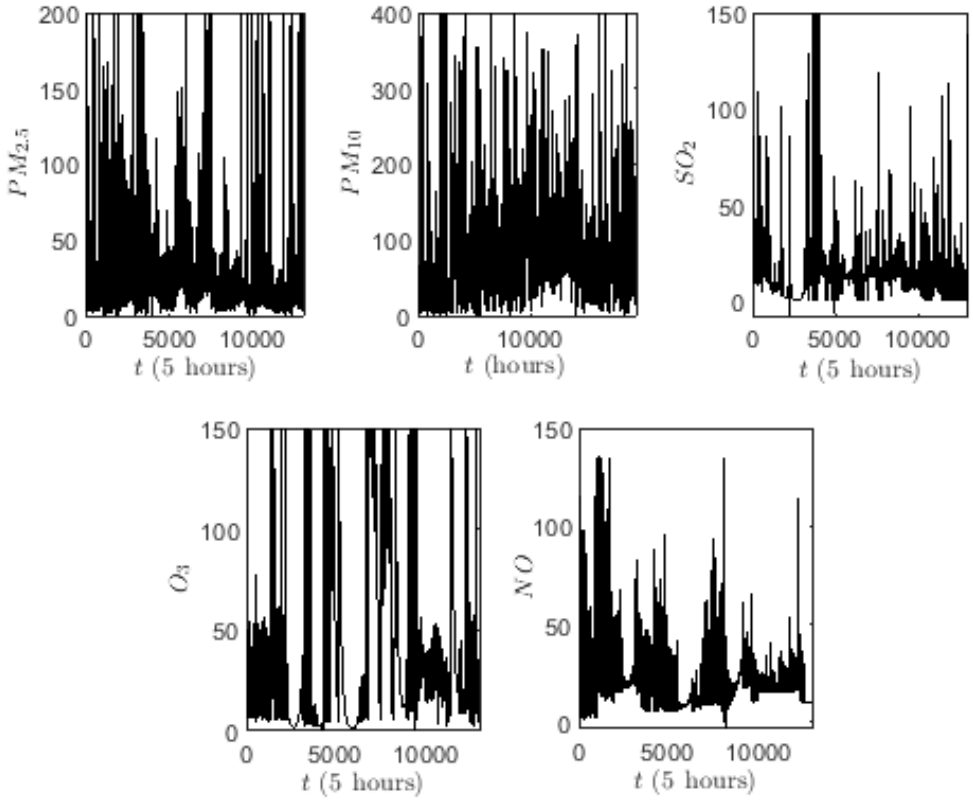


FIGURE 2. Air pollutants concentration levels in Khorram Abad after some preprocessing operations.

- Evaluating the results: To demonstrate the efficiency of MSNN, we compare the results with several well-known neural model. To evaluate the model performance, MSE is used.

Although this study primarily focuses on air pollution forecasting using data from Khorramabad, the proposed MSNN framework is designed to generalize effectively to other locations and environmental conditions. The use of Sinc basis functions enables the network to capture both periodic and irregular fluctuations that are common in atmospheric pollutant data across different regions, while the Lyapunov-based learning algorithm ensures stable parameter adaptation even when the statistical properties of the data change. To examine this capability, we performed the experiments by training the model on some segments of data and testing it on unseen data. Nonetheless, we acknowledge that further

evaluation using datasets from multiple cities and diverse climatic zones would provide a more comprehensive understanding of the model's external generalizability. Such future experiments are planned to confirm the scalability and robustness of MSNN for nationwide or global air quality forecasting applications.

5. **Air pollution forecasting using the MSNN**

In this section, MSNN is used for forecasting air pollutant concentration levels by utilizing information from air pollution monitoring stations in Khorram Abad, Iran. The input vector for the models is defined as $X_k = [x_k, x_{k-1}, x_{k-2}]^T$.

TABLE 2. MSEs of neural models in the forecasting of $PM_{2.5}$ pollutant concentration.

Model	n_h	h	No. of Parameters	A	Γ_i	Testing MSE
MLP	80	-	400	-190	$0.05I_{80}$	4.65e-4
SNN	-	0.1	31	-190	$2I_{31}$	7.11e-4
MSNN	-	0.1	34	-190	$2I_{34}$	**2.96e-4**

5.1. **Forecasting of $PM_{2.5}$ pollutant concentration.** The forecasting of $PM_{2.5}$ pollutant concentration was carried out using three neural network architectures: MLP, SNN, and MSNN. For the MLP, trainable parameters were initialized randomly within the range $[-3, 3]$, whereas in the SNN and MSNN models, the initialization interval was set to $[-5, 5]$ to account for the different basis functions and parameter sensitivities inherent to these architectures. The choice of initialization range was guided by preliminary sensitivity tests, which indicated that broader intervals allow Sinc-based models to capture oscillatory components of the time series more effectively. Additional hyper-parameters, such as learning rate Γ_i, number of hidden neurons n_h, and linear part matrix A, are summarized in Table 2.

To provide a fair comparison, all models were trained on the same dataset split (90% training, and 10% testing) and evaluated under identical stopping criteria. The performance was assessed using the MSE. As reported in Table 2, the MSNN consistently achieved lower MSE value compared with both MLP and SNN. The comparative forecasting results of MLP and MSNN for $PM_{2.5}$ are illustrated in Figure 3. It can be observed

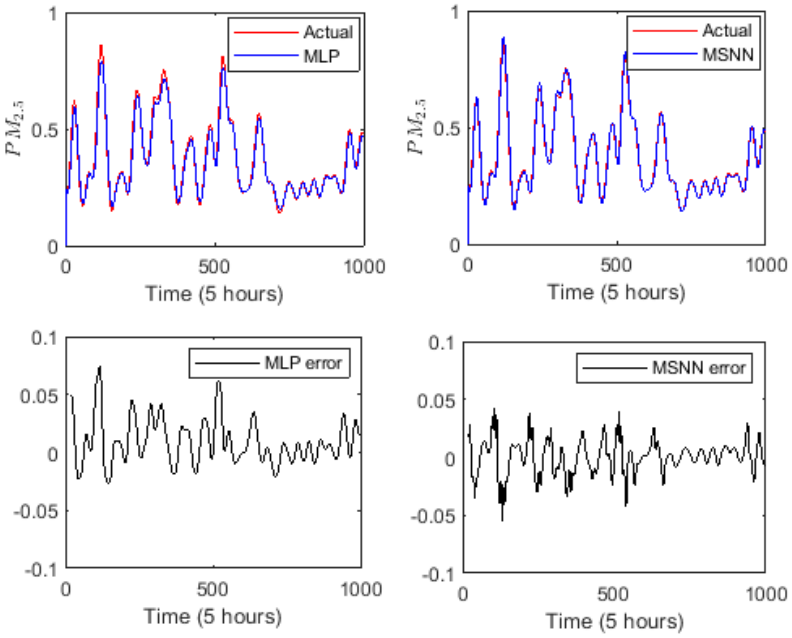


FIGURE 3. Implementation of MLP and MSNN to forecast the concentration level of $PM_{2.5}$.

that MSNN captures the trends more accurately, especially during high-pollution episodes where MLP tends to underestimate the peaks.

Overall, the analysis demonstrates that the MSNN achieves superior predictive accuracy despite its relatively simple architecture and fewer trainable parameters. These results underscore the efficiency of the proposed model and highlight its potential for real-world applications in environmental time series forecasting. In addition, the inclusion of both tabular results (Table 2) and graphical comparisons (Figure 3) provides a more comprehensive evaluation of model behavior, thereby strengthening the validity of the findings.

5.2. **Forecasting of PM_{10} pollutant concentration.** The forecasting of PM_{10} pollutant concentration was carried out using three neural network architectures: MLP, SNN, and MSNN. For the MLP, trainable parameters were initialized randomly within the range $[-5, 5]$, whereas in the SNN and MSNN models, the initialization interval was set to $[-0.5, 0.5]$ to account for the different basis functions and parameter sensitivities

TABLE 3. MSEs of neural models in the forecasting of PM_{10} pollutant concentration.

Model	n_h	h	No. of Parameters	A	Γ_i	Testing MSE
MLP	85	-	505	-55	$0.01I_{80}$	2.68e-4
SNN	-	0.1	31	-65	$0.3I_{31}$	2.36e-4
MSNN	-	0.1	34	-65	$0.3I_{34}$	**1.75e-4**

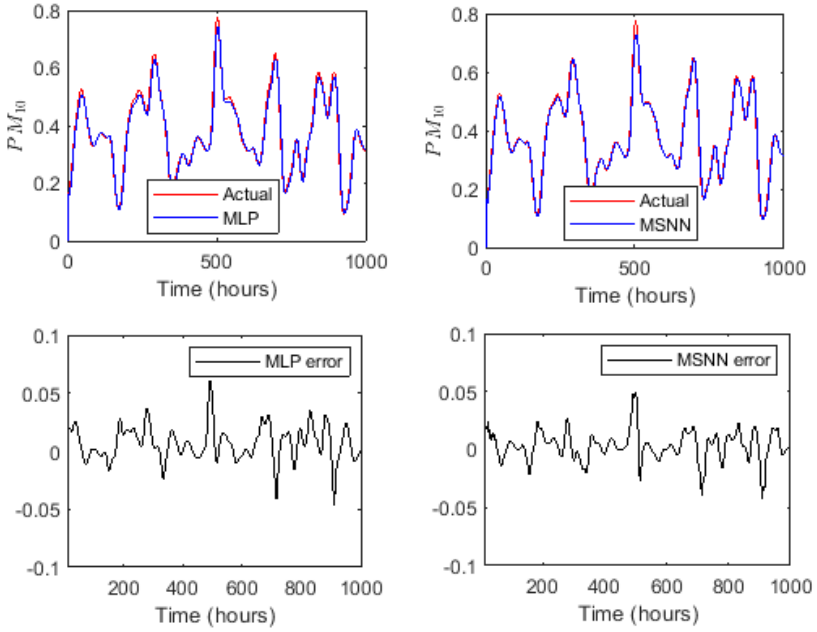


FIGURE 4. Implementation of MLP and MSNN to forecast the concentration level of PM_{10}.

inherent to these architectures. Additional hyper-parameters, such as learning rate Γ_i, number of hidden neurons n_h, and linear part matrix A, are summarized in Table 3.

To provide a fair comparison, all models were trained on the same dataset split (90% training, and 10% testing) and evaluated under identical stopping criteria. The performance was assessed using the MSE. As reported in Table 3, the MSNN consistently achieved lower MSE value compared with both MLP and SNN. The comparative forecasting results of MLP and MSNN for PM_{10} are illustrated in Figure 4. It can be observed

that MSNN captures the trends more accurately, especially during high-pollution episodes where MLP tends to underestimate the peaks.

Overall, the analysis demonstrates that the MSNN achieves superior predictive accuracy despite its relatively simple architecture and fewer trainable parameters. These results underscore the efficiency of the proposed model and highlight its potential for real-world applications in environmental time series forecasting. In addition, the inclusion of both tabular results (Table 3) and graphical comparisons (Figure 4) provides a more comprehensive evaluation of model behavior, thereby strengthening the validity of the findings.

TABLE 4. MSEs of neural models in the forecasting of NO pollutant concentration.

Model	n_h	h	No. of Parameters	A	Γ_i	Testing MSE
MLP	70	-	350	-60	$0.01I_{80}$	4.05e-5
SNN	-	0.2	16	-60	$0.4I_{31}$	1.48e-4
MSNN	-	0.2	19	-60	$0.4I_{34}$	**2.88e-5**

5.3. **Forecasting of NO pollutant concentration.** The forecasting of NO pollutant concentration was carried out using three neural network architectures: MLP, SNN, and MSNN. For the MLP, trainable parameters were initialized randomly within the range $[-5, 5]$, whereas in the SNN and MSNN models, the initialization interval was set to $[-15, 15]$ to account for the different basis functions and parameter sensitivities inherent to these architectures. The choice of initialization range was guided by preliminary sensitivity tests, which indicated that broader intervals allow Sinc-based models to capture oscillatory components of the time series more effectively. Additional hyper-parameters, such as learning rate Γ_i, number of hidden neurons n_h, and linear part matrix A, are summarized in Table 4.

To provide a fair comparison, all models were trained on the same dataset split (90% training, and 10% testing) and evaluated under identical stopping criteria. The performance was assessed using the MSE. As reported in Table 4, the MSNN consistently achieved lower MSE value compared with both MLP and SNN. The comparative forecasting results of MLP and MSNN for NO are illustrated in Figure 5. It can be observed

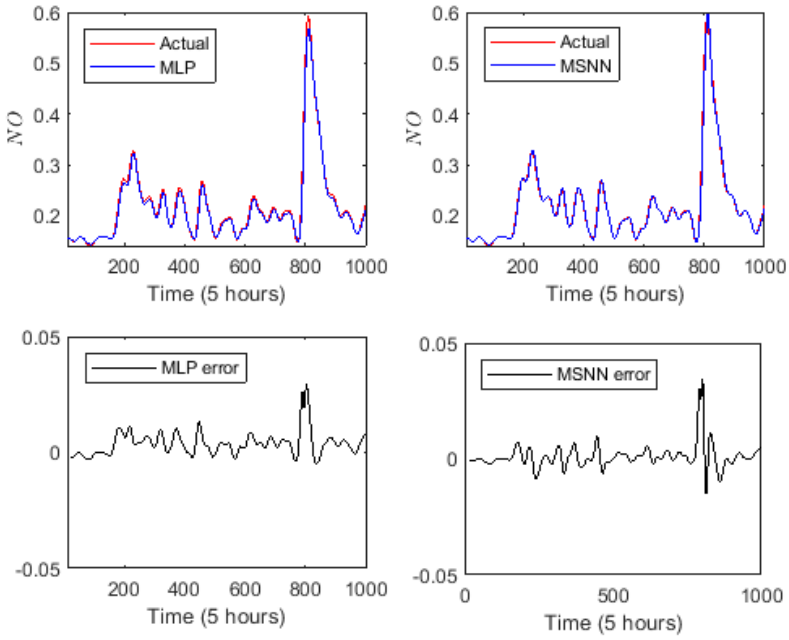


FIGURE 5. Implementation of MLP and MSNN to forecast the concentration level of NO.

that MSNN captures the trends more accurately, especially during high-pollution episodes where MLP tends to underestimate the peaks.

Overall, the analysis demonstrates that the MSNN achieves superior predictive accuracy despite its relatively simple architecture and fewer trainable parameters. These results underscore the efficiency of the proposed model and highlight its potential for real-world applications in environmental time series forecasting. In addition, the inclusion of both tabular results (Table 4) and graphical comparisons (Figure 5) provides a more comprehensive evaluation of model behavior, thereby strengthening the validity of the findings.

5.4. **Forecasting of SO_2 pollutant concentration.** The forecasting of SO_2 pollutant concentration was carried out using three neural network architectures: MLP, SNN, and MSNN. For the MLP, trainable parameters were initialized randomly within the range $[-4.5, 4.5]$, whereas in the SNN and MSNN models, the initialization interval was set to $[-0.025, 0.025]$ to account for the different basis functions and parameter sensitivities

TABLE 5. MSEs of neural models in the forecasting of SO_2 pollutant concentration.

Model	n_h	h	No. of Parameters	A	Γ_i	Testing MSE
MLP	85	-	505	-55	$0.01I_{80}$	7.44e-5
SNN	-	0.2	16	-55	I_{16}	1.80e-4
MSNN	-	0.2	19	-55	$0.2I_{19}$	**6.47e-5**

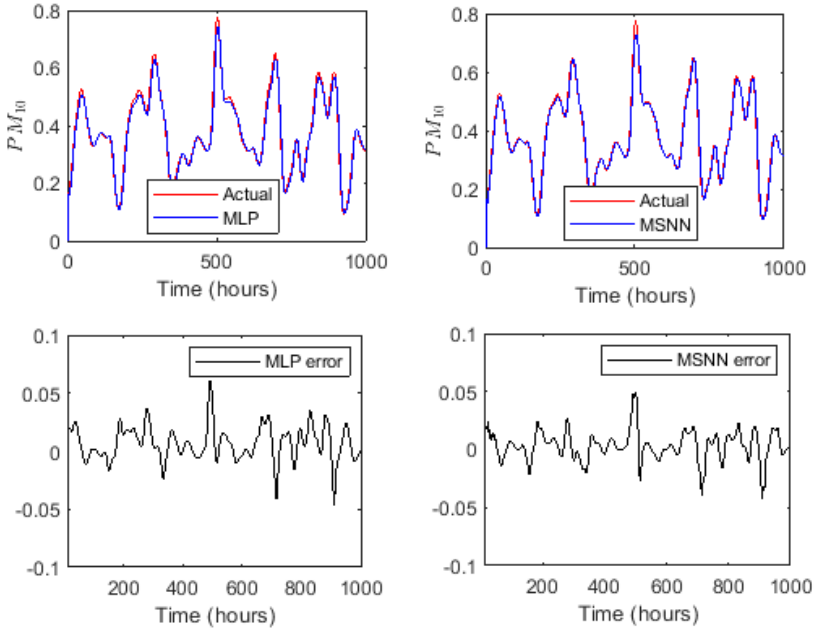


FIGURE 6. Implementation of MLP and MSNN to forecast the concentration level of SO_2.

inherent to these architectures. Additional hyper-parameters, such as learning rate Γ_i, number of hidden neurons n_h, and linear part matrix A, are summarized in Table 5.

To provide a fair comparison, all models were trained on the same dataset split (90% training, and 10% testing) and evaluated under identical stopping criteria. The performance was assessed using the MSE. As reported in Table 5, the MSNN consistently achieved lower MSE value compared with both MLP and SNN. The comparative forecasting results of MLP and MSNN for SO_2 are illustrated in Figure 6. It can be observed

that MSNN captures the trends more accurately, especially during high-pollution episodes where MLP tends to underestimate the peaks.

Overall, the analysis demonstrates that the MSNN achieves superior predictive accuracy despite its relatively simple architecture and fewer trainable parameters. These results underscore the efficiency of the proposed model and highlight its potential for real-world applications in environmental time series forecasting. In addition, the inclusion of both tabular results (Table 5) and graphical comparisons (Figure 6) provides a more comprehensive evaluation of model behavior, thereby strengthening the validity of the findings.

TABLE 6. MSEs of neural models in the forecasting of O_3 pollutant concentration.

Model	n_h	h	No. of Parameters	A	Γ_i	Testing MSE
MLP	80	-	400	-60	$0.01I_{80}$	8.68e-6
SNN	-	0.1	31	-60	$0.3I_{31}$	6.62e-5
MSNN	-	0.1	34	-60	$0.3I_{34}$	**4.44e-6**

5.5. **Forecasting of O_3 pollutant concentration.** The forecasting of O_3 pollutant concentration was carried out using three neural network architectures: MLP, SNN, and MSNN. For the MLP, trainable parameters were initialized randomly within the range $[-5, 5]$, whereas in the SNN and MSNN models, the initialization interval was set to $[-15, 15]$ to account for the different basis functions and parameter sensitivities inherent to these architectures. The choice of initialization range was guided by preliminary sensitivity tests, which indicated that broader intervals allow Sinc-based models to capture oscillatory components of the time series more effectively. Additional hyper-parameters, such as learning rate Γ_i, number of hidden neurons n_h, and linear part matrix A, are summarized in Table 6.

To provide a fair comparison, all models were trained on the same dataset split (90% training, and 10% testing) and evaluated under identical stopping criteria. The performance was assessed using the MSE. As reported in Table 6, the MSNN consistently achieved lower MSE value compared with both MLP and SNN. The comparative forecasting results of MLP and MSNN for O_3 are illustrated in Figure 7. It can be observed

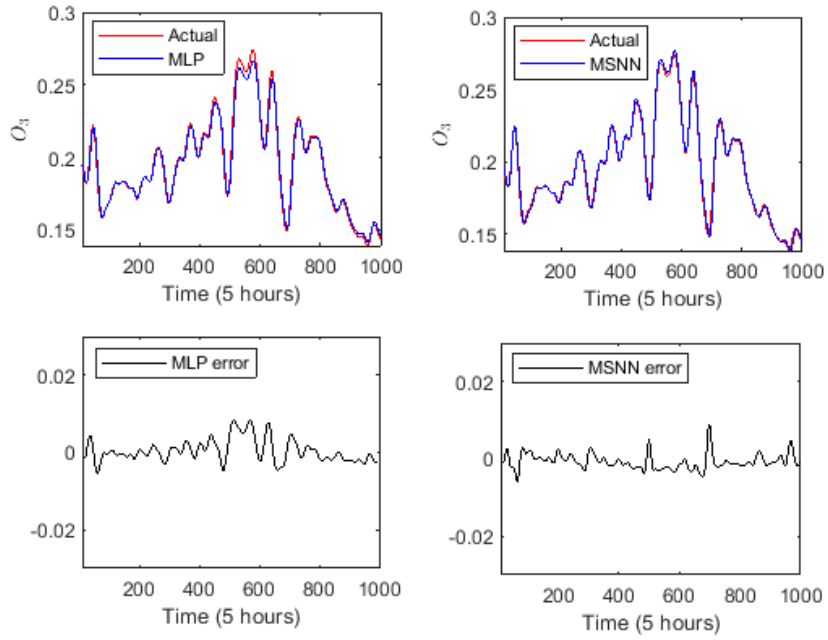


FIGURE 7. Implementation of MLP and MSNN to forecast the concentration level of O_3.

that MSNN captures the trends more accurately, especially during high-pollution episodes where MLP tends to underestimate the peaks.

Overall, the analysis demonstrates that the MSNN achieves superior predictive accuracy despite its relatively simple architecture and fewer trainable parameters. These results underscore the efficiency of the proposed model and highlight its potential for real-world applications in environmental time series forecasting. In addition, the inclusion of both tabular results (Table 6) and graphical comparisons (Figure 7) provides a more comprehensive evaluation of model behavior, thereby strengthening the validity of the findings.

6. **Conclusion**

This study underscores the critical challenge of air pollution in Khorram Abad, Iran, and highlights the innovative application of the modified Sinc neural network (MSNN) for predicting pollutant concentration levels. Despite its relatively simple architecture and fewer trainable parameters, MSNN has demonstrated superior performance compared to

traditional multilayer perceptron (MLP), and standard Sinc neural network (SNN) models. By integrating advanced modeling techniques with real-time learning algorithms, this research provides a robust foundation for informed urban management and the development of effective pollution mitigation strategies. The ability to accurately forecast air pollution levels can significantly aid policymakers in implementing timely interventions, thereby reducing the adverse health and environmental impacts associated with poor air quality. In the future, research could be directed toward broadening the dataset to include a wider range of detailed and diverse air quality indicators, as well as incorporating emerging technologies such as deep learning and hybrid models. These advancements could further enhance the accuracy and reliability of air pollution forecasts, ultimately leading to more effective and targeted policy interventions. Additionally, exploring the integration of MSNN with other machine learning frameworks and real-time data streams could open new avenues for dynamic and adaptive air quality management systems.

Acknowledgments

The author of this article extends his deepest gratitude to the managers and staff of the meteorological and environmental organizations in Khorram Abad for their invaluable cooperation and support in providing the essential data used in this study.

References

[1] Ahmadi, G., 2024. Using a modified Sinc neural network to identify chaotic systems with an application in wind speed forecasting. *Journal of Mathematical Modeling*, **12**(4), pp. 733–752. doi:10.22124/jmm.2024.27752.2442

[2] Ahmadi, G., 2022. Stochastic gradient-based hyperbolic orthogonal neural networks for nonlinear dynamic systems identification. *Journal of Mathematical Modeling*, **10**(3), pp. 529–547. doi:10.22124/jmm.2022.19635.1884

[3] Ahmadi, G., 2025. Applying the Modified Sinc Neural Network for Weather Forecasting. *Journal of Data Science and Modeling*, **3**(1), pp. 1–28. doi:10.22054/jdsm.2025.84908.1065

[4] Ahmadi, G. and Akbari, Z., 2024. Investigating air pollutants in Lorestan Province and predicting their concentration using a multilayer neural network with stable online training (case studies: Khorramabad and Poldokhtar). *Nivar*, **48**(126–127), pp. 109–126. doi:10.30467/nivar.2024.464234.1296

[5] Ahmadi, G. and Dehghandar, M., 2023. Chaotic time series prediction using rough-neural networks. *Mathematics in Interdisciplinary Research*, **8**(2), pp. 71–92. doi:10.22052/MIR.2023.242878.1290

[6] G. Ahmadi, M. Teshnehlab and F. Soltanian, A higher order online Lyapunov-based emotional learning for rough-neural identifiers, *Control and Optimization in Applied Mathematics* **3** (2018), no. 1, 87–108. doi:10.30473/COAM.2019.40779.1083

[7] Biswas, S., Ayna, C.O., Gurbuz, S.Z. and Gurbuz, A.C., 2023. CV-SincNet: Learning complex sinc filters from raw radar data for computationally efficient human motion recognition. *IEEE Transactions on Radar Systems*, **1**, pp. 493–504. doi:10.1109/TRS.2023.3310894

[8] Borra, D., Fantozzi, S. and Magosso, E., 2020. Interpretable and lightweight convolutional neural network for EEG decoding: Application to movement execution and imagination. *Neural Networks*, **129**, pp. 55–74. doi:10.1016/j.neunet.2020.05.032

[9] Bria, A., Marrocco, C. and Tortorella, F., 2021. Sinc-based convolutional neural networks for EEG-BCI-based motor imagery classification. In: Del Bimbo, A. et al. (eds.) *Pattern Recognition. ICPR International Workshops and Challenges*. Lecture Notes in Computer Science, Vol. 12661. Cham: Springer, pp. 91–103. doi:10.48550/arXiv.2101.10846

[10] Chen, J., Lu, J., Avise, J. and DaMassa, J., 2014. Seasonal modeling of $PM_{2.5}$ in California's San Joaquin Valley. *Atmospheric Environment*, **92**, pp. 182–190. doi:10.1016/j.atmosenv.2014.04.030

[11] Cordova, C.H., Portocarrero, M.N.L., Salas, R. et al., 2021. Air quality assessment and pollution forecasting using artificial neural networks in Metropolitan Lima, Peru. *Scientific Reports*, **11**, Article 24232. doi:10.1038/s41598-021-03650-9

[12] Dong, J., Zhang, Y. and Hu, J., 2024. Short-term air quality prediction based on EMD-Transformer-BiLSTM. *Scientific Reports*, **14**, Article 20513. doi:10.1038/s41598-024-67626-1

[13] Eftekhari, A. and Saadatmandi, A., 2021. DE Sinc-collocation method for solving a class of second-order nonlinear boundary value problems. *Mathematics in Interdisciplinary Research*, **6**(1), pp. 11–22. doi:10.22052/mir.2020.220050.1195

[14] Elwasif, W. and Fausett, L.V., 1996. Function approximation using a sinc neural network. In: *Proceedings of SPIE*, Vol. 2760, pp. 690–701. doi:10.1117/12.235959

[15] Ghaemi, Z., Taleai, M., Farnaghi, M., Javadi, G., 2017. Prediction of air pollution in Tehran city using the combination of fuzzy-adaptive neural network and principal component analysis, *Iranian Remote Sensing and GIS Journal*, *3*(9), pp.45-70 [In persian].

[16] Heydari Dastjerdi, R. and Ahmadi, G., 2024. Designing sinc neural networks to solve fractional optimal control problems. *Iranian Journal of Numerical Analysis and Optimization*, **14**(4), pp. 1016–1036. doi:10.22067/ijnao.2024.86494.1380

[17] Ioannou, P., Sun, J., 1996. *Robust Adaptive Control*, Prentice Hall, New Jersey.

[18] Liu, K., Yang, M., Xing, X., Yu, Z. and Wu, W., 2023. SincMSNet: A sinc-filter convolutional neural network for EEG motor imagery classification. *Journal of Neural Engineering*, **20**(5), Article 056024. doi:10.1088/1741-2552/acf7f4

[19] Luo, J. and Gong, Y., 2023. Air pollutant prediction based on ARIMA-WOA-LSTM model. *Atmospheric Pollution Research*, **14**(6), Article 101761. doi:10.1016/j.apr.2023.101761

[20] Ma, Z., Wang, B., Luo, W. et al., 2024. Air pollutant prediction model based on transfer learning two-stage attention mechanism. *Scientific Reports*, **14**, Article 7385. doi:10.1038/s41598-024-57784-7

[21] Maleki, H., Sorooshian, A., Goudarzi, G., Baboli, Z. and Rahmati, M., 2019. Air pollution prediction using an artificial neural network model. *Clean Technologies and Environmental Policy*, **21**, pp. 1341–1352. doi:10.1007/s10098-019-01709-w

[22] Nandi B.P., Singh G, Jain A. and Tayal D.K., 2023. Evolution of neural network to deep learning in prediction of air, water pollution and its Indian context. *International Journal of Environmental Science and Technology. 29*, pp. 1–16. doi:10.1007/s13762-023-04911-y

[23] Parcollet, T., Morchid, M. and Linares, G., 2020. E2E-SincNet: Toward fully end-to-end speech recognition. In: *Proceedings of ICASSP 2020*, Barcelona, Spain. doi:10.1109/ICASSP40776.2020.9053954

[24] Radha, K., Bansal, M. and Pachori, R.B., 2024. Automatic speaker and age identification of children from raw speech using SincNet over ERB scale. *Speech Communication*, **159**, Article 103069. doi:10.1016/j.specom.2024.103069

[25] Rashki, A., Middleton, N.J. and Goudie, A.S., 2021. Dust storms in Iran: Distribution, causes, frequencies and impacts. *Aeolian Research*, **48**, Article 100655. doi:10.1016/j.aeolia.2020.100655

[26] Sadeghi, H., Khaksar Astane, S. 2015. Short-term prediction of air pollution in Ahvaz city with the help of neural networks, *Environmental Research*, *5*(9), pp.177-186. [In persian]

[27] Saide, P., et al., 2011. Forecasting urban PM_{10} and $PM_{2.5}$ pollution episodes in very stable nocturnal conditions and complex terrain using WRF–Chem CO tracer model. *Atmos. Environ.*, *45*, pp.2769–2780. doi:10.1016/j.atmosenv.2011.02.001

[28] Schanze, T., 1995. Sinc interpolation of discrete periodic signals. *IEEE Transactions on Signal Processing*, **43**(6), pp. 1502–1503. doi:10.1109/78.388863

[29] Seinfeld, J.H., Pandis, S.N., 1997. *Atmospheric Chemistry and Physics: From Air Pollution to Climate Change*, Wiley-VCH: New York.

[30] Stenger, F., 2010. *Handbook of Sinc Numerical Methods*. Boca Raton, FL: CRC Press.

[31] Teng, M., Li, S., Xing, J., Fan, C. and Yang, J. et al., 2023. 72-hour real-time forecasting of ambient $PM_{2.5}$ using a hybrid graph deep neural network with aggregated neighborhood spatiotemporal information. *Environment International*, **176**, Article 107971. doi:10.1016/j.envint.2023.107971

[32] Tiwary, A., Williams, I. and Colls, J., 2018. *Air Pollution: Measurement, Modelling and Mitigation*. 4th ed. Boca Raton, FL: CRC Press.

Ghasem Ahmadi
Department of Mathematics,
Payame Noor University,
Tehran, Iran
Email: g.ahmadi@pnu.ac.ir

©2024 Shahid Chamran University of Ahvaz, Ahvaz, Iran. This article is an open-access article distributed under the terms and conditions of the Creative Commons Attribution-NonComertial 4.0 International (CC BY-NC 4.0 license) (http://creativecommons.org/licenses/by-nc/4.0/).